

Stars and gas in the very large interacting galaxy NGC 6872

C. Horellou¹ and B. Koribalski²

¹ Onsala Space Observatory, Chalmers University of Technology, SE-439 92 Onsala, Sweden
e-mail: Cathy.Horellou@chalmers.se

² Australia Telescope National Facility, CSIRO, P.O. Box 76, Epping, NSW 1710, Australia
e-mail: Baerbel.Koribalski@csiro.au

Received 13 July 2006 / Accepted 2 November 2006

ABSTRACT

The dynamical evolution of the large (> 100 kpc), barred spiral galaxy NGC 6872 and its small companion IC 4970 in the southern group Pavo is investigated. We present N -body simulations with stars and gas and 21 cm H I observations carried out with the Australia Telescope Compact Array of the large-scale distribution and kinematics of atomic gas. H I is detected toward the companion, corresponding to a gas mass of $\sim 1.3 \times 10^9 M_{\odot}$. NGC 6872 contains $\sim 1.4 \times 10^{10} M_{\odot}$ of H I gas, distributed in an extended rotating disk. Massive concentrations of gas ($\sim 10^9 M_{\odot}$) are found at the tip of both tidal tails and towards the break seen in the optical northern arm near the companion. We detect no H I counterpart to the X-ray trail between NGC 6872 and NGC 6876, the dominant elliptical galaxy in the Pavo group located $\sim 8'$ to the southeast. At the sensitivity and the resolution of the observations, there is no sign in the overall H I distribution that NGC 6876 has affected the evolution of NGC 6872. There is no evidence of ram pressure stripping either. The X-ray trail could be due to gravitational focusing of the hot gas in the Pavo group behind NGC 6872 as the galaxy moves supersonically through the hot medium. The simulations of a gravitational interaction with a small nearby companion on a low-inclination prograde passage are able to reproduce most of the observed features of NGC 6872, including the general morphology of the galaxy, the inner bar, the extent of the tidal tails and the thinness of the southern tail.

Key words. galaxies: interaction – galaxies: ISM – ISM: kinematics and dynamics – galaxies: individual: NGC 6872, IC 4970, NGC 6876

1. Introduction

Galaxies with extended tidal tails form an outstanding laboratory to study the effect of a collision on the different components of a galaxy because of the sensitivity of the morphology and kinematics of the tails to the initial distribution of the matter (both luminous and dark) and to the geometry of the interaction (e.g., Dubinski et al. 1999, Springel & White 1999). Early simulations clearly showed that prograde, co-planar encounters are more efficient than retrograde encounters at triggering long thin tails (e.g., Holmberg 1941, Pfeiderer & Siedentopf 1961, Pfeiderer 1963, Toomre & Toomre 1972). The tails are made of stars and gas that have been thrown out from the galactic disks during the gravitational interaction which may lead to the merger of the two disks. Spectacular examples of nearby galaxies at different stages of an interaction can be found in the Arp atlas (1966) and the Arp & Madore catalog (1987). The tails are often gas-rich and their kinematics can be traced out to large radii by 21 cm line observations of atomic hydrogen (e.g., Hibbard & van Gorkom 1996). Some tidal tails contain massive self-gravitating concentrations of matter which may be the progenitors of the so-called tidal dwarf galaxies (Elmegreen et al. 1993, Bournaud et al. 2003, Bournaud et al. 2004). Tidal tails develop not only in merging systems, but also in flyby encounters, where the interacting galaxies do not form a bound system. It is of particular interest to study tidal tails at an early time of the interaction when the two galaxies are well separated and have a clear morphology. A few 10^7 yr after closest approach, the tails are already well developed and it is possible to reconstruct the

dynamical history of the interaction and examine its influence on the different components of a galaxy and the level of induced star formation.

The southern galaxy NGC 6872 is one of the largest spiral galaxies known. Star formation is traced all along the arms, which extend over more than 100 kpc at our adopted distance of 61 Mpc. The galaxy belongs to a small group, Pavo (see Fig. 1a). NGC 6872 is likely to be affected by tidal perturbations from the nearby companion IC 4970, a small lenticular galaxy located 1:1 to the north. Machacek et al. (2005) have discovered a more than 100 kpc long X-ray trail extending between NGC 6872 and the neighbor galaxy NGC 6876, the dominant elliptical in the group which lies about $8'$ (~ 142 kpc) to the southeast. The radial velocity of NGC 6876 is about 800 km s^{-1} lower than that of NGC 6872 (see Table 1). The X-ray trail is hotter (~ 1 keV) than the undisturbed Pavo intergalactic medium (~ 0.5 keV) and has a low metal abundance. The authors interpret the trail as partly due to gravitational focusing of the intracluster gas into a Bondi-Hoyle wake, as the spiral galaxy moves supersonically through the intracluster medium; they point out that the trail could also consist of a mixture of intracluster gas and gas removed from NGC 6872 by turbulent viscous stripping.

The spectacular Very Large Telescope (VLT) multicolor image of NGC 6872/IC 4970 displays striking contrasts between the inner region, especially the straight northern arm, and the blue diffuse tidal tail to the north-east (ESO Press Release 20b/99; see also Fig. 1b, which shows the VLT blue-band image on a grey scale). A bar is clearly seen in the 2MASS J, H, K images (Jarrett et al. 2003). Fabry-Pérot $H\alpha$ observations have revealed the presence of ionized gas at the tip of both tails

	Note NGC 6872	IC 4970	NGC 6876
Other names	ESO 073-IG 32 VV 297a AM 2011-705	ESO 073-IG 33 VV 297b	ESO 073-IG035
α (J2000)	(1) 20 ^h 16 ^m 56.91	20 ^h 16 ^m 57.87	20 ^h 18 ^m 19.15
δ (J2000)	(1) -70°46′04″.5	-70°44′57″.3	-70°51′31″.7
Type	(2) .SBS3P.	.LA.-P*	SB0
Systemic velocity	(2) 4818 km s ⁻¹	4727 km s ⁻¹	4010 km s ⁻¹
Distance	(3) 61 Mpc		
Scale	17.75 kpc arcmin ⁻¹ 296 pc arcsec ⁻¹		
D_{25}	(2) 6′.025=106.9 kpc	0′.676=12 kpc	2′.8
Position angle	(2) 66°	6°	79°
Axis ratio	(2) 0.288=cos(73°)	0.323=cos(71°)	0.786=cos(38°)
$f_{60\mu\text{m}}$	(4) 1.67 Jy		
$f_{100\mu\text{m}}$	(4) 6.61 Jy		
T_{FIR}	(4) 28 K		
L_{FIR}	(4) $1.6 \times 10^{10} L_{\odot}$		
L_B	(2) $1.67 \times 10^{11} L_{\odot}$	$1.24 \times 10^{10} L_{\odot}$	$1.07 \times 10^{11} L_{\odot}$
H I mass	(5) $1.41 \times 10^{10} M_{\odot}$	$1.3 \times 10^9 M_{\odot}$	
H ₂ mass	(6) $9.6 \times 10^8 M_{\odot}$		

Notes: (1) Position of NGC 6872: Russell et al. (1990), uncertainty of 2′.5. Position of IC 4970: Lauberts (1982), uncertainty of 7′.5. Position of NGC 6876: Skrutskie et al. (2006), uncertainty of 1′.25. (2) Systemic velocity of NGC 6876: Davoust & Considere (1995); other data: de Vaucouleurs et al. (1991). The blue-band luminosities have been derived from the blue-band magnitudes corrected for extinction, B_T^0 , using the following relation: $\log(L_B/L_{\odot}) = 12.192 - 0.4B_T^0 + \log(D/1\text{Mpc})^2$, consistent with the blue magnitude for the Sun $M_B^0 = 5.48$.

(3) Consistent with $H_0 = 75 \text{ km s}^{-1} \text{ Mpc}^{-1}$.

(4) Moshir & et al. (1990). The far-infrared luminosity L_{FIR} , in solar luminosities, has been derived from the flux densities at 60 and 100 μm listed in the IRAS catalogue using the relation: $L_{\text{FIR}} = 3.94 \times 10^5 D^2 (2.58f_{60} + f_{100})$ where D is the distance in Mpc, f_{60} and f_{100} are the flux densities in Jy. The dust temperature T_{FIR} has been derived from f_{60} and f_{100} by fitting a black body and assuming that the dust emissivity is inversely proportional to the wavelength.

(5) This work.

(6) Horellou & Booth (1997). The H₂ mass refers to the central 45″ of NGC 6872 and was derived from CO(1-0) observations using a standard CO-H₂ conversion factor.

Table 1. Basic parameters of NGC 6872/IC 4970.

(Mihos et al. 1993). The location of the ionized regions coincides with that of young, blue stellar clusters seen in the optical images. No H α emission was detected from the central region and the bar, nor from the early-type companion IC 4970.

Bastian et al. (2005) have studied the rich population of star clusters in NGC 6872 using archival VLT images in the B , V , and I bands, complemented with new VLT observations in the U -band. They estimated the mass, age and extinction of the star clusters and found that most of the young massive clusters (of mass between 10^4 and $10^7 M_{\odot}$ and less than 100 Myr old) are located in the tidal tails or in the outer part of the galactic disk. The mass distribution of the star clusters follows a power-law with an index similar to that found in other galaxies. The authors also estimated the star formation rate in different regions of the galaxy and showed that the northern tail is forming stars at about twice the rate of the southern tail, and about five times the rate of the main body.

Mihos et al. (1993) have modeled the dynamic evolution of NGC 6872, as it is gravitationally perturbed during the passage of the small companion IC 4970 on a low-inclination, prograde orbit. They were able to reproduce most of the observed features, although the simulated tidal tails were not as thin as the observed ones. The model predicted an accumulation of gas toward the center, which was subsequently detected in CO emission (Horellou & Booth 1997).

In this paper, we present new maps of the large-scale distribution and kinematics of atomic hydrogen (H I) in the NGC 6872/IC 4970 system and N -body simulations with stars and gas. With a total H I mass $> 1.5 \times 10^{10} M_{\odot}$ (Horellou & Booth

1997, 1999), the pair is among the most gas-rich galaxies in the optically selected sample of ~ 60 interacting and merging galaxies compiled by Johansson & Bergvall (1990). The single-dish H I spectrum is extremely broad ($\sim 950 \text{ km s}^{-1}$ at the base of the H I line) and observations at a resolution higher than the Parkes 15′ beam were required to determine the location of the H I gas. The Australia Telescope Compact Array (ATCA) in several configurations makes it possible to obtain data with angular resolution ($\sim 40''$, corresponding to about $\sim 12 \text{ kpc}$ at our adopted distance) and a sensitivity adequate to detect extended H I emission. We pointed the array half-way between the large spiral galaxy and NGC 6876, the dominant elliptical in the Pavo group located ca 8′ to the south-east, in order to be more sensitive to diffuse H I gas in the Pavo group and detect traces of a possible gravitational interaction in the extended H I distribution.

We also discuss N -body simulations with stars and gas performed using a particle-mesh code, where the gas is modeled as a collection of clouds that dissipate energy through inelastic collisions. Preliminary results have been presented elsewhere (Horellou & Koribalski 2003, Horellou & Koribalski 2004). We have used simulations to investigate the evolution of gas and stars in such a close encounter, examine the influence of the dark matter halo and of the geometry of the collision on the characteristics of the tidal tails and place constraints on the dynamical history of the observed system.

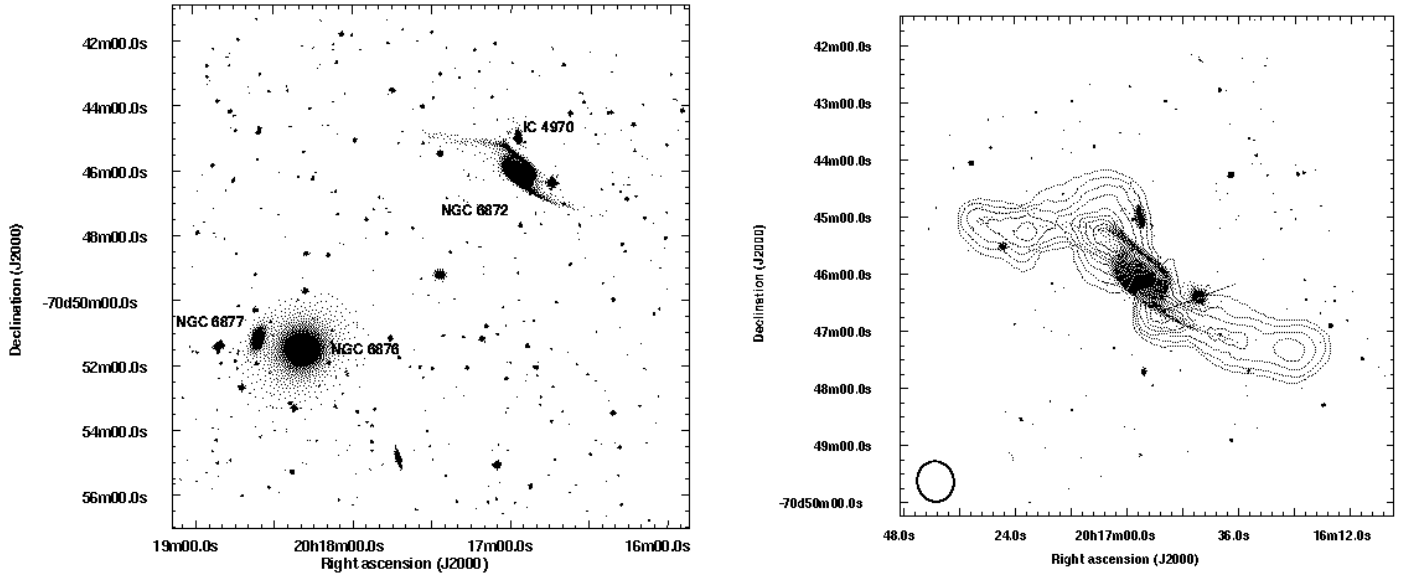


Fig. 1. (a) Optical image from the Digitized Sky Survey of the field around NGC 6872. North is up and east is left. Machacek et al. (2005) detected diffuse X-ray emission in the region between NGC 6872 and the massive elliptical galaxy NGC 6876. (b) Integrated HI map overlaid on the blue-band VLT image. The contour levels increase from $14.4 \times 10^{19} \text{ cm}^{-2}$ to $115.4 \times 10^{19} \text{ cm}^{-2}$ by steps of $14.4 \times 10^{19} \text{ cm}^{-2}$. The synthesized beam is shown in the bottom left corner. The frame is 155 kpc on each side for the adopted distance.

2. HI Observations

2.1. Observations and data reduction

HI observations were carried out using the ATCA in five different configurations. Details are given in Table 2. The correlator provided a total bandwidth of 16 MHz divided in 512 channels, which corresponds to a total velocity coverage of 3431 km s^{-1} and a velocity resolution of 6.7 km s^{-1} . The data were reduced in MIRIAD and AIPS using standard procedures. After substantial flagging (narrow-band interferences around 1400, 1403 and 1406 MHz plus broad-band solar interference, all affecting the shortest baselines) the data were calibrated using PKS 1934–638 which lies only 8° away from NGC 6872. The 20-cm continuum emission was subtracted by fitting a first order base level to all line-free channels. The four good HI line data sets were then Fourier-transformed together using ‘robust’ weighting (ROBUST=0.5). To enhance the signal-to-noise ratio of the HI emission we smoothed the data to a velocity resolution of $\sim 20 \text{ km s}^{-1}$. All velocities are in the barycentric reference frame using the optical definition. The final maps obtained by combining the various data sets have a synthesised beam of $42''.4 \times 38''.8$ and a noise level per channel of 0.90 mJy, which is very close to the theoretical value of 0.85 mJy. Moment maps (zeroth order, first and second order) were obtained using signals above 2 mJy beam^{-1} .

HI masses are related to the HI integrated intensities $\int S_{\text{HI}} dv$ (in Jy km s^{-1}) by:

$$M(\text{HI})(M_{\odot}) = 2.36 \times 10^5 D_{\text{Mpc}}^2 \int S_{\text{HI}} dv \quad (1)$$

where D_{Mpc} is the distance to the galaxy in Mpc.

HI column densities can be derived from the observed integrated intensities by using the relation:

$$N_{\text{HI}} = \frac{110.4 \times 10^3}{ab} \int S_{\text{HI}} dv \quad (2)$$

Arrays,	750D, 25/09/2001, 12h
observing dates	1.5D (corrupt), 17/11/2001, <6h
and durations	EW352, 26/12/2001, 12h
	1.5B, 07/07/2002, 12h
	750B, 03/08/2002, 12h
Pointing position (J2000)	$20^{\text{h}}17^{\text{m}}38^{\text{s}}; -70^{\circ}48'47''$
Primary beam	$34''.1$
Central frequency	1399 MHz
Number of channels	512
Calibrator	PKS 1934–638 (14.91 Jy)
Combined data:	
Synthesized beam	
- Major \times minor axis	$42''.4 \times 38''.8$ (FWHM)
- Position angle	$+12^\circ$
Channel width	$\Delta v = 20.55 \text{ km s}^{-1}$
Noise level (1σ)	$0.9 \text{ mJy beam}^{-1} \text{ channel}^{-1}$
	$1.24 \times 10^{19} \text{ cm}^{-2} \text{ channel}^{-1}$
	$1.6 \times 10^7 M_{\odot} \text{ beam}^{-1} \text{ channel}^{-1}$

Table 2. Summary of HI observations.

where N_{HI} is the column density of hydrogen atoms in 10^{19} cm^{-2} and a and b are the diameters of the synthesized beam at full width half maximum (FWHM) in arcseconds.

2.2. Results

2.2.1. HI distribution

Figures 1b and 2 display the HI distribution as isocontours superimposed on the blue-band VLT image on a grey scale. The atomic gas is confined to the interacting galaxies NGC 6872/IC 4970 and there is no evidence for the presence of extended HI gas around the galaxies or in the region between NGC 6872 and the massive elliptical NGC 6876. We measure an HI flux of $17.5 \text{ Jy km s}^{-1}$ toward NGC 6872/IC 4970, which is less than the published single-dish measurements within

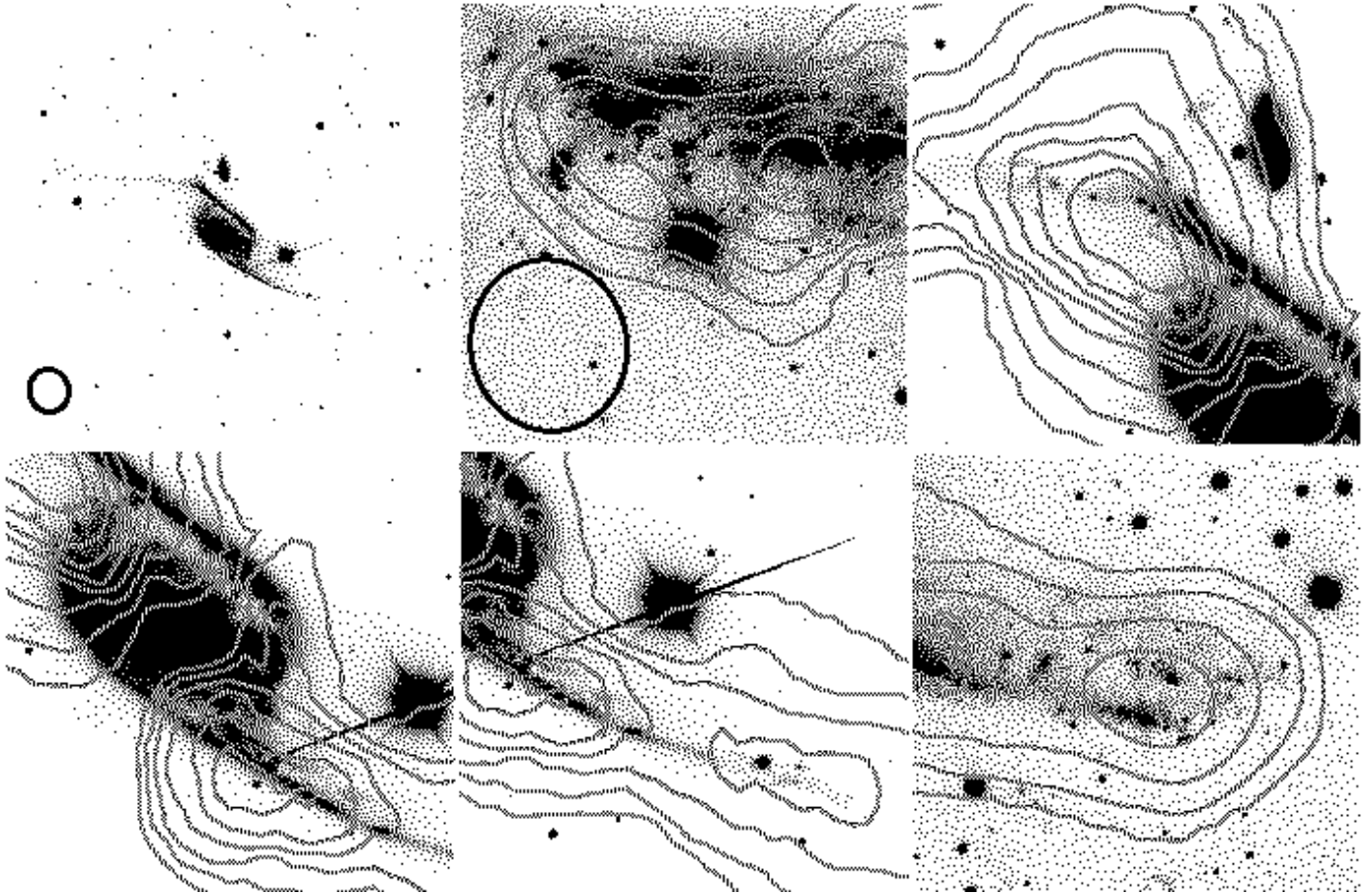


Fig. 2. Details of the H I distribution as contours overlaid on the VLT B-band image, as in the previous figure. The size of the beam is indicated in the lower left corner of the first two frames. Aside from the first frame, all the other frames have the same size. North is up and east is left. The contour levels are the same as in the previous figure. In Figure 4 the H I concentrations in the southern tail are labeled S1 to S3 and those in the northern tail N1 and N2. Their H I content is given in Table 3.

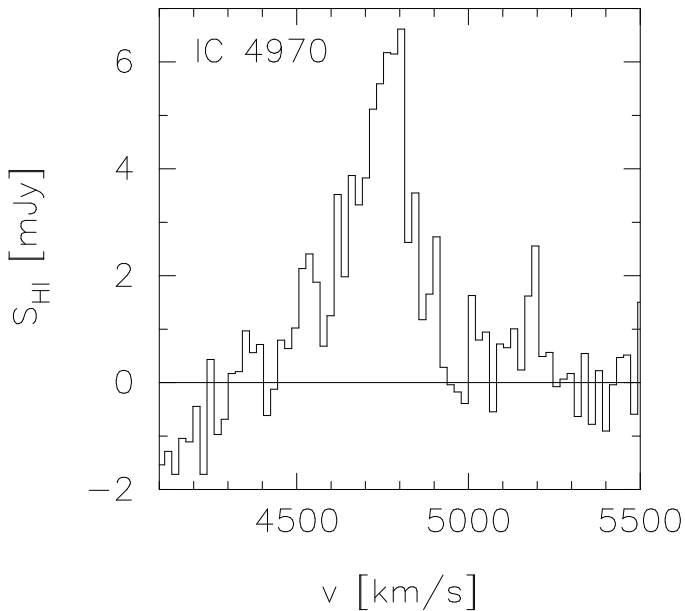


Fig. 3. H I spectrum toward the companion IC 4970.

the 15' beam of the Parkes antenna: $20.1 \pm 0.5 \text{ Jy km s}^{-1}$ (Horellou & Booth 1997); $21.7 \text{ Jy km s}^{-1}$ (Meyer et al. 2004, en-

try HIPASS J2016-770 in the HICAT catalog). Since the single-dish flux is around 21 Jy km s^{-1} , as much as $\sim 3.5 \text{ Jy km s}^{-1}$ could be distributed in an extended area outside the main galaxies and below the detection limit of our interferometric observations. This corresponds to as much as $\sim 3 \times 10^9 M_{\odot}$ of H I gas, or 20% the amount of H I gas contained in the NGC 6872/IC 4970 system. We can also use the noise level in our maps to estimate the H I flux in the area of the X-ray trail, which Machacek et al. (2005) define as a $4'.35 \times 5'.9$ rectangular region between the NGC 6872 and the large elliptical NGC 6876. This area is about 50 times larger than our synthesized beam. From the noise level given in Table 1, we can estimate the noise equivalent flux density in that area as $NEFD = \sqrt{50}\sigma \approx 6.4 \text{ mJy}$. The radial velocity difference between the two galaxies is $\Delta v \sim 800 \text{ km s}^{-1}$, which gives a flux $NEFD \times \Delta v = 5.1 \text{ Jy km s}^{-1}$. This value is clearly too high since it exceeds the difference between the interferometric and the single-dish measurements.

The central region of NGC 6872 is devoid of atomic gas. H I was found neither in absorption toward the central continuum source, nor in emission. This is not unusual in spiral galaxies, where most of the gas in the center is often in molecular form. From observations of the CO(J:1-0) line toward the center of NGC 6872, Horellou & Booth (1997) inferred a mass of molecular hydrogen $M(H_2)$ of $9.6 \times 10^8 M_{\odot}$ within the central $45''$.

The companion galaxy, IC 4970, is clearly detected in H I (Fig. 3). It contains $\sim 1.3 \times 10^9 M_{\odot}$ of atomic gas.

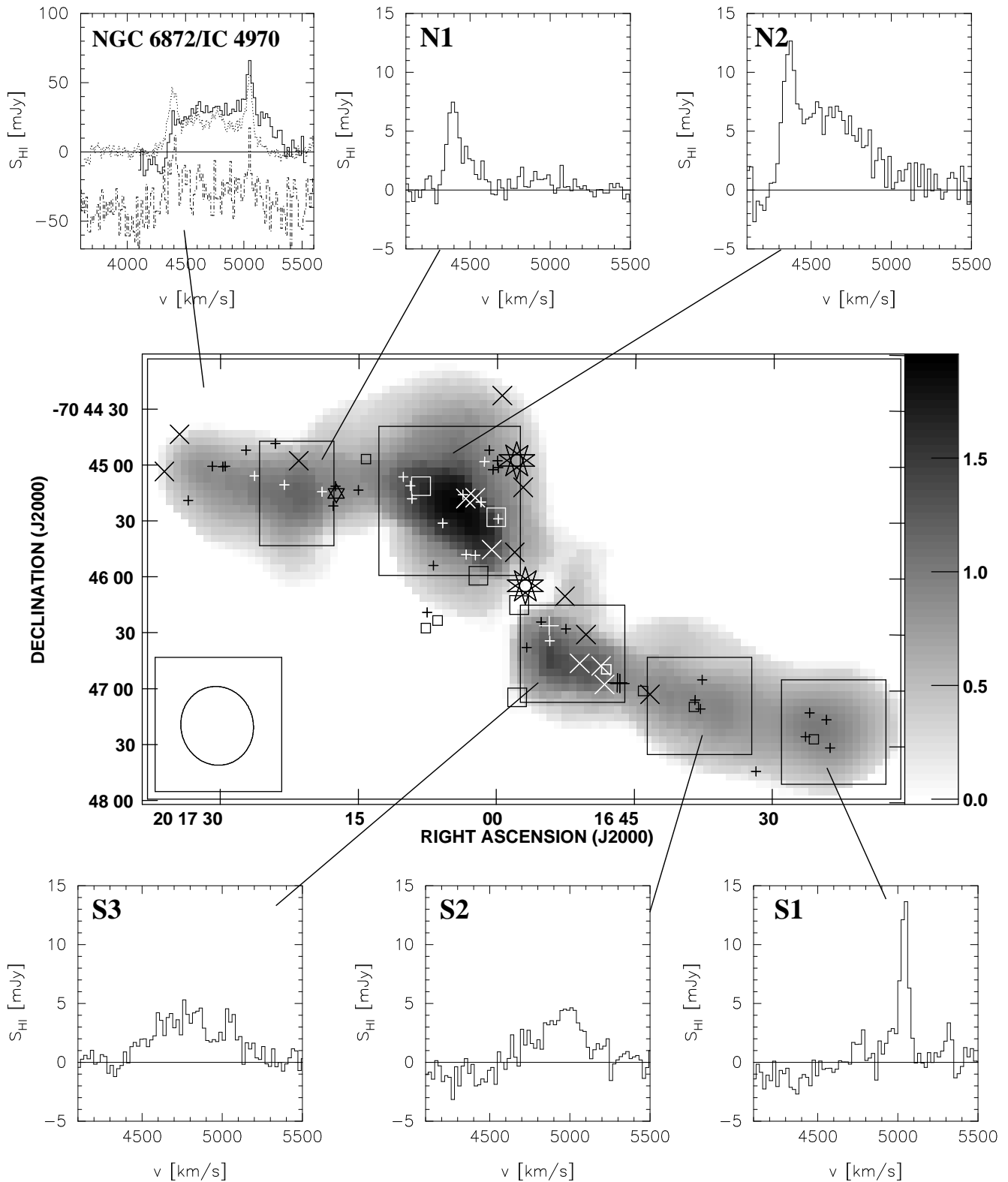


Fig. 4. Grey-scale map of the HI distribution and HI spectra measured over several regions in the tails labeled S1, S2 and S3 (southern concentrations) and N1 and N2 (northern concentrations). The first spectrum was measured in the rectangular area around the NGC 6872/IC 4970 system. The solid line refers to the ATCA observations, the dotted line is the single-dish Parkes spectrum of Horellou & Booth (1997) and the dotted-dashed line is the Parkes HIPASS spectrum, which has been shifted by -40 mJy for clarity. The ten-pointed stars mark the positions of the centers of NGC 6872 and of IC 4970. The location of the star clusters detected by Bastian et al. (2005) is indicated. Star clusters less massive than $10^6 M_{\odot}$ are marked by small symbols, and more massive clusters by large symbols. Plus signs and squares correspond to star clusters younger than 100 Myr, and crosses and stars of David to older clusters. The squares and stars of David indicate a large extinction, with $A_V > 1$. Note that the regions S1 and S2 at the tip of the southern tail contain only young star clusters.

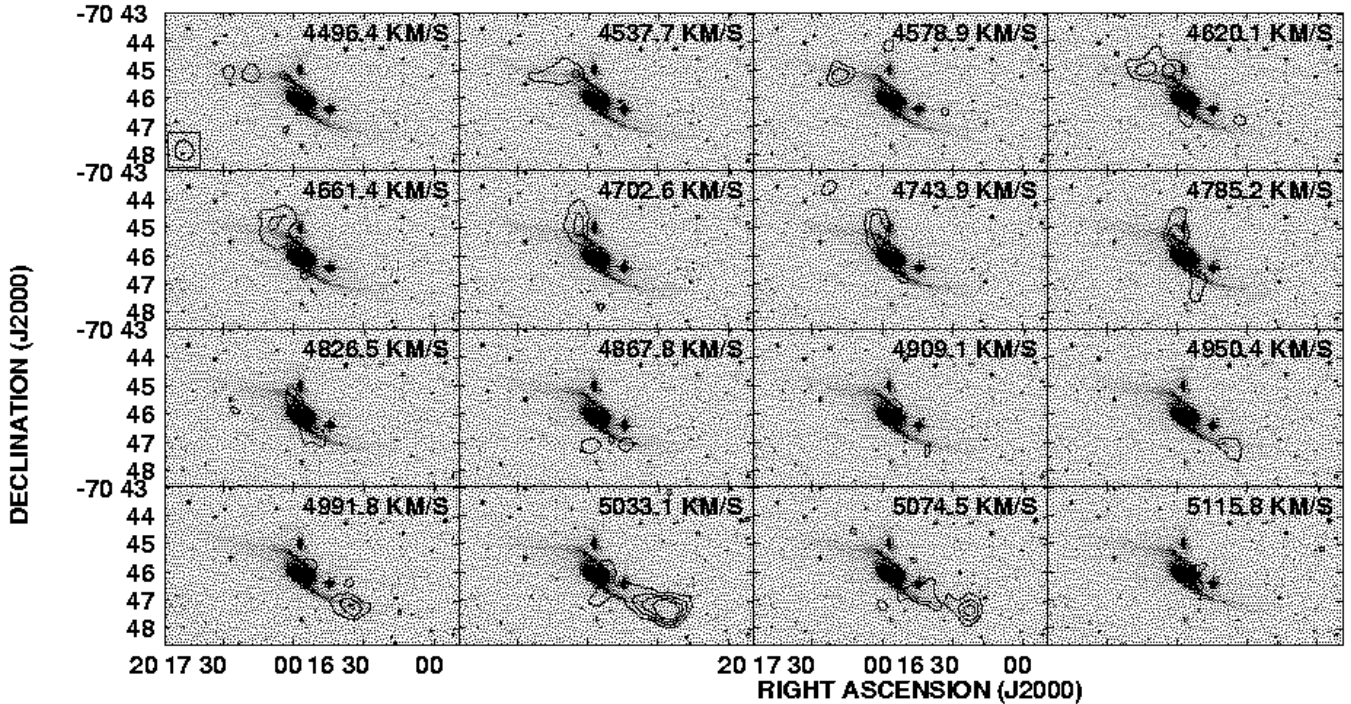


Fig. 5. The HI emission of NGC 6872 overlaid on a grey scale optical image from the Digitized Sky Survey and displayed as channel maps running from 4496 km s⁻¹ (top left panel) to 5116 km s⁻¹ (bottom right panel). Every other channel is shown of the channel maps showing HI emission. North is up and east is left. The levels are 3, 5, 7, 9 mJy/beam. The first contour corresponds to the $\sim 3\sigma$ level. The synthesized beam is shown in the bottom left corner of the first panel.

Five large HI concentrations are seen in the outer parts of NGC 6872, two in the northern tail and three in the southern one. Figure 2 shows that the most northern concentration is spatially roughly coincident with blue stellar clusters. This is also where peaks in the H α distribution were seen (Mihos et al. 1993). A significant amount of HI is also found near the break in the northern arm, close to the nearby companion IC 4970. In the southern tail, the three HI peaks all occur in regions where star clusters are seen in the blue-band image.

There is a clear overall asymmetry in the HI distribution: we estimate that the north-eastern part contains about 1.4 times as much atomic gas as the south-western part. Bastian et al. (2005) estimated a star formation rate of $\sim 16.5 M_{\odot}\text{yr}^{-1}$ in the north-eastern tail and about half that amount in the western tail, using an empirical relationship between the specific *U*-band luminosity and the star formation rate measured by Larsen & Richtler (2000). In the center, they inferred a star formation rate about five times lower than in the north-eastern tail.

Finally, we show integrated HI spectra measured in different regions of the galaxy, as illustrated in Figure 4. The regions in the southern tail have been labeled S1 to S3, and those in the northern tail N1 and N2. The amount of gas contained in each region is given in Table 3. Gas at the tip of the southern tail in region S1 produces a narrow HI line (width ~ 100 km s⁻¹) centered around 5050 km s⁻¹. Emission from the other regions produces broader spectra. In region N2, which lies near the break in the northern arm, there are clearly several velocity components. Region N1 near the tip of the northern arm also exhibits a narrow HI line.

The global HI spectrum integrated over the whole NGC 6872/IC 4970 system is shown in Fig. 4 (first spectrum, upper left). The line is very broad (~ 950 km s⁻¹ at the base), in agreement with the Parkes single-dish HI spectra (Horellou & Booth 1997, Meyer et al. 2004), also shown in

Fig. 4. Since Horellou & Booth (1997) used the radio convention $v_{\text{rad}}/c = \Delta v/v$ for velocities, we converted the values to show the spectrum using the optical definition $v_{\text{opt}}/c = \Delta\lambda/\lambda$ used in the present paper. The low-velocity peak around 4400 km/s seen in the single-dish HI spectra is not seen in the ATCA map.

Also shown in Fig. 4 is the location of the star clusters detected by Bastian et al. (2005). We have divided the star clusters into different groups, depending on their age (more or less than 100 Myr), mass (more or less than $10^6 M_{\odot}$), and extinction (more or less than $A_v = 1$), using the estimates of Bastian et al. (2005) based on the three dimensional spectral energy fitting algorithm of Bik et al. (2003). Interestingly, clusters in the outer regions of the tails (S1, S2, N1, and the region at the very tip of the northern tail) are predominantly young and low-mass and have a low extinction (small plus signs). Some old, low extinction massive clusters (larger crosses) are found north of the northern tail at the border of the HI distribution. Such old massive clusters are also found in the inner region (regions S3 and N3). Several young, low-mass, low-extinction clusters (small plus signs) are found near the companion, slightly to the east, and it is likely that their formation has been triggered in the interaction. Regions S3 and N1 contain large amounts of HI gas, and a collection of star clusters. The young ones (plus signs and boxes) seem to lie at the periphery of the HI concentrations. There is no systematic indication that clusters with higher extinction (boxes) lie closer to the peak of the HI concentration. Star clusters are expected to form from denser, molecular gas which does not necessarily coincide with the more diffuse atomic gas observed here. Also, some clusters may lie in the front part of the HI concentration and not suffer from much extinction. Bastian et al. (2005) found an excellent correlation between the location of the youngest clus-

Region	$\int S_{\text{HI}} dv$ Jy km s ⁻¹	$M(\text{HI})$ M _⊙	d kpc
NGC 6872/IC 4970	17.5	1.54×10^{10}	
NGC 6872	16.0	1.41×10^{10}	
IC 4970	1.46	1.3×10^9	
N1	1.25	1.1×10^9	17
N2	4.40	3.9×10^9	39
S1	2.18	1.9×10^9	53
S2	1.03	0.90×10^9	34
S3	0.86	0.75×10^9	12

Table 3. HI fluxes and corresponding HI masses. The values for NGC 6872 were obtained by subtracting those measured toward the companion from the values measured for the pair. The third column lists the distance on the sky of the peak of the various HI concentrations labeled in Fig. 4 to the center of NGC 6872.

ters (< 10 Myr) and the distribution of H α emission in the map of Mihos et al. (1993).

2.2.2. HI kinematics

We now examine the kinematical information that can be gained from the HI maps. Figure 5 shows the velocity channel maps as isovelocity contours superimposed on an optical image. Gas in the north-eastern tail has a lower velocity along the line-of-sight (an heliocentric velocity around 4500 km s⁻¹) than the south-western tail (around 5100 km s⁻¹). The line-of-sight velocities vary smoothly across the galaxy and are characteristic of those of a rotating disk.

Figure 6 shows the mean HI velocity field (top) and the HI velocity dispersion (bottom). Again, the smooth velocity gradient across the galaxy appears clearly. The velocity dispersion map shows a peak on each side of the galaxy's center. One is located on the concave side near the break of the northern arm. The other one lies south of the main body of the galaxy where the southern tail begins. A region of increased velocity dispersion (~ 75 km s⁻¹) coincides with the N1 HI concentration in the northern tail.

3. N-body simulations

In order to narrow down the parameter space we first used a restricted three-body model. 10 000 test particles were distributed in a Miyamoto potential representing a galactic disk. The particles were advanced according to the gravitational effect of the potential of the host galaxy and that of a perturbing companion represented by a rigid Plummer potential moving on a Keplerian orbit. A good match was found for a prograde, parabolic, low-inclination encounter with a companion five times less massive than the primary, in agreement with the findings of Mihos et al. (1993). Then we carried out self-consistent simulations with stars and gas, as described below.

3.1. The model

The simulations were performed using a particle-mesh algorithm (FFT3D) that makes use of the properties of Fast Fourier Transforms and of the convolution theorem. The gravitational potential is calculated at the nodes of a three-dimensional 128 \times 128 \times 64 cartesian grid, providing a resolution of 1 kpc. Effective use is made of the entire grid, rather than of only one eighth

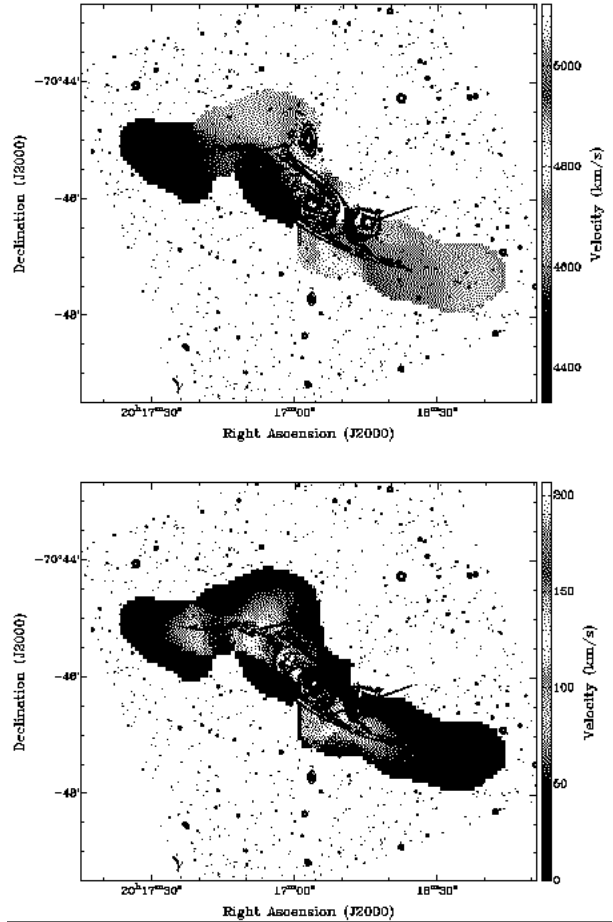


Fig. 6. Top: HI velocity field in colors superimposed on the VLT blue-band image in contours. Bottom: HI velocity dispersion map in colors superimposed on the VLT blue-band image in contours.

in standard Fourier algorithms, through implementation of a method described by James (1977).

The main galaxy is made up of three components: a disk, a bulge, and a halo. The halo is rigid and represented by a Plummer potential, $\Phi(r) = GM/(r^2 + a^2)^{1/2}$. The bulge contains particles initially distributed in a Plummer potential. The disk contains two types of particles with different velocity dispersions. The collisionless particles representing the stars are initially distributed in a Toomre-Kuzmin disk so that the surface density has the radial dependence $\Sigma(R) = M_G b / [2\pi(R^2 + b^2)^{3/2}]$. The vertical density profile corresponds to that of an isothermal sheet $\rho(z) \propto 1/ch^2(z/z_0)$ (Spitzer 1942). The gaseous component is modeled as an ensemble of clouds, all of the same mass, that dissipate energy through inelastic collisions with each other. Gas clouds approaching each other inside a cell collide and exchange energy every tenth time step (every 10⁷ year). Initially, the gas follows a flat radial distribution and accounts for about 10% of the mass of the stellar disk. The self-gravity of the gas is taken into account. Initially, the particles are assigned circular velocities in centrifugal equilibrium with the gravitational potential, and velocity dispersions are given by Toomre's stability criterion (Toomre 1964).

The companion galaxy is modeled as a rigid body represented by a Plummer potential. The assumption of a rigid structure for the companion is justified insofar as we are interested

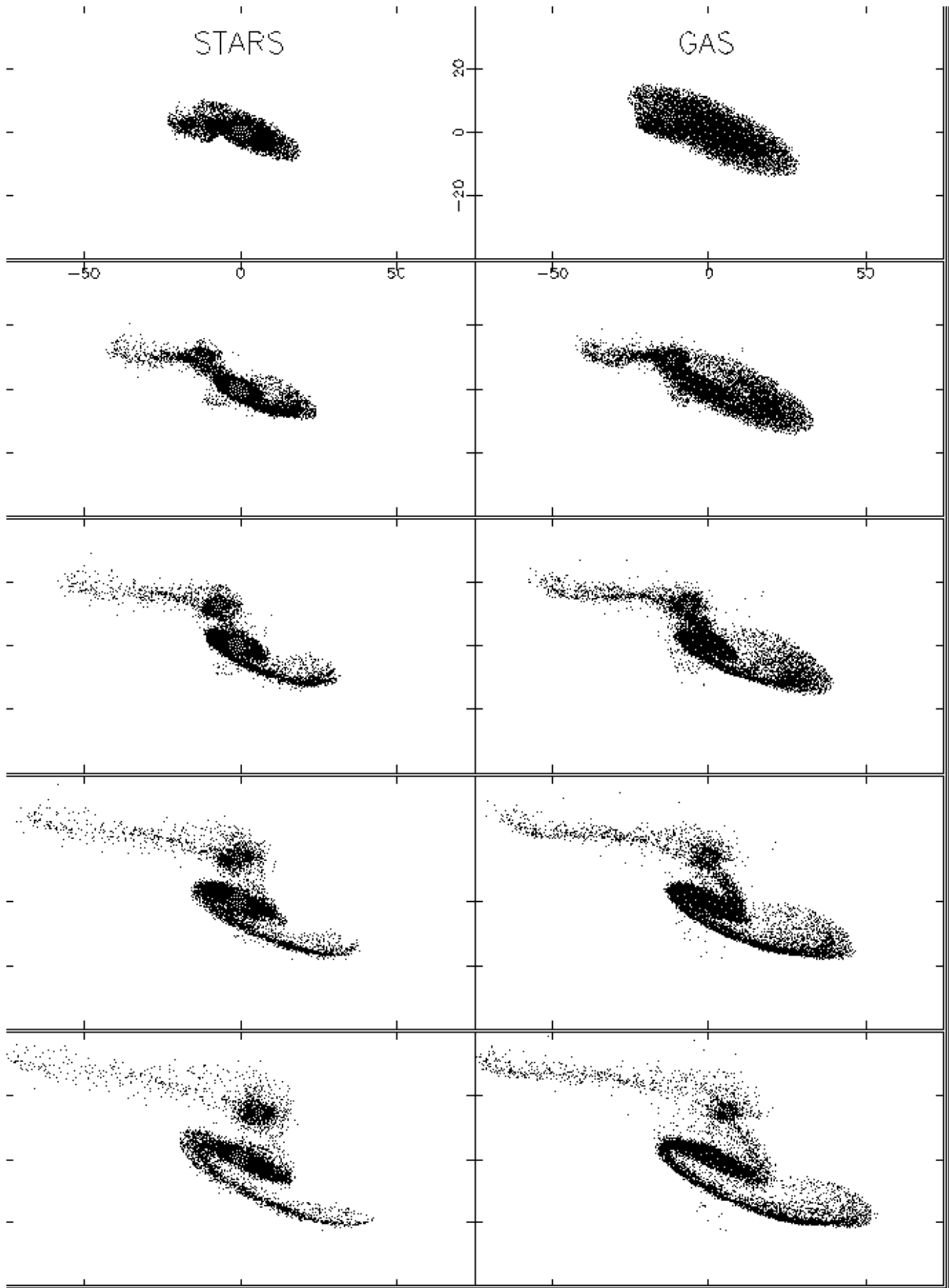


Fig. 7. Evolution of the stars (left column) and the gas (right column) in the simulation of NGC 6872/IC 4970. The stars in the bulge of the primary galaxy are shown in red. The system is viewed according to the observed geometry (position angle of 66° , inclination of 73°). The time step between two snapshots is 40 Myr, starting 20 Myr after perigalacticon. The position of the companion is indicated by a star.

Orbit	Parabolic
Mass ratio	5:1
Main galaxy: mass and scale length	$M_{\text{disk}} = 120, a_{\text{disk}} = 3$ $M_{\text{bulge}} = 30, a_{\text{bulge}} = 0.45$ $M_{\text{halo}} = 90, a_{\text{halo}} = 10$
orientation	$(15^\circ, 315^\circ)$
Companion: mass and scale length	$M_c = 48, a_c = 1$

Table 4. Parameters of the simulations. The orientation of the main galaxy is given by the angle between the orbital plane and the galactic plane (15°) and the angle between the x -axis in the orbital plane and the projection of the vector normal to the main galaxy onto the orbital plane.

in the effect of its passage on the internal structure of the larger galaxy, which is probably little affected by the distortion of the companion.

Setting the units of length and time to 1 kpc and 10^7 years, with the gravitational constant G set to 1, gives a unit of mass of $2.22 \times 10^9 M_\odot$. The time step was set to 10^6 years, and particles were advanced using the leap-frog algorithm. We used 440 000 particles to model the disk and the bulge of the primary galaxy (25% of the particles being initially attributed to the bulge) and 60 000 gas cloud particles. The parameters of the simulation presented here are listed in Table 4.

3.2. Results

Figure 7 displays the evolution of the stars and the gas in the primary galaxy as it is perturbed by the companion passing on a prograde, parabolic orbit. The gas distribution is initially more extended than that of the stars. The time between two snapshots is 40 Myr, starting 20 Myr after closest approach. Despite its small mass (one fifth of the mass of the primary), the companion triggers prominent tidal tails very rapidly. The southern tail on the side of the galaxy opposite to the companion is thinner than the northern tail, where the perturbation is stronger. In the simulation the companion, modeled as a rigid Plummer potential and displayed by a red star, accretes significant amounts of matter (both stars and gas). In the observed system, some diffuse stellar emission is seen between the companion and the northern arm of the primary, but it is not clear that stars or gas have been dragged or have fallen onto the companion. Also, in the simulation the northern arm breaks at the location of the companion, whereas in the observed system both galaxies appear more clearly separated. Aside from those differences, the model is able to reproduce several observed features, including the extent of the tidal tails, the thinness of the southern tail, the central bar, the relative position of the two galaxies. The simulated system resembles the observed one most around 130 Myr after closest approach, as shown in Fig. 8. For that epoch, we also display the velocities of the gas in the simulations (over the whole galaxy in Fig. 9 and in the inner part in Fig. 10). The arrows indicate the direction of the velocity of the gas on the plane of the sky, whereas the colors are related to the velocities along the line-of-sight. The line-of-sight velocities are in good agreement with the observed velocity field. Interestingly, the simulation shows that gas in the outer part of the northern tail moves outward, whereas gas in the inner part moves inward toward the companion.

The results of our simulations generally agree with those of Mihos et al. (1993). The gas is modeled in a similar way, as sticky particles, although in our simulation all gas clouds keep the same mass and do not evolve by coalescence or fragmenta-

tion. Star formation is not included in our model either. The initial conditions are slightly different: in our simulation, the orbital plane of the companion is slightly less inclined on the galactic plane (15° instead of 25°); their simulated halo is four times more massive than the stellar disk, whereas the spherical components of our model are less massive (the added mass of the bulge and of the halo is the same as that of the disk). This is why the tidal tails are slightly longer and thinner in our simulation. We find a blueshift of the companion relative to the main galaxy (-192 km s^{-1}), as Mihos et al. (1993) who found -130 km s^{-1} . The true velocity difference between the two galaxies is uncertain since the published observations cover a large range of values: For the companion, Green et al. (1988) measured 4759 km s^{-1} , while RC3 give 4727 km s^{-1} . For NGC 6872, the following values are quoted: 4626 (Green et al. 1988), 4688 (Meyer et al. 2004, H α spectrum), 4717 (Horellou & Booth 1997, H α spectrum), 4818 (RC3); 4892 km s^{-1} (Horellou & Booth 1997, CO spectrum). For comparison we converted the velocities quoted by Horellou & Booth (1997) in the radio convention $\Delta v/v$ to the more commonly used optical convention $\Delta\lambda/\lambda$. The broad range of velocities across NGC 6872 (more than 900 km s^{-1} at the base of the single-dish H α spectrum) makes it difficult to accurately measure the systemic velocity. Taking the value from the CO spectrum of NGC 6872, which traces the molecular gas in the central $45''$, and the RC3 value for the companion gives a blueshift for the companion of -165 km s^{-1} , roughly consistent with the simulations.

Within our model, the various parameters are well constrained by the characteristic morphology of the observed system and we did not find a significantly different set of parameters that would give an equally good match to the observations. This, however, could change with the addition of more parameters in the model (e.g. a halo spin or a different density profile, or an additional gravitational perturbation due, for instance, to a third galaxy).

4. Discussion

Machacek et al. (2005) discuss several possibilities to explain the diffuse X-ray emission seen between NGC 6872 and the large elliptical galaxy NGC 6876.

– As they argue, it is unlikely that the hot gas has been extracted from the elliptical galaxy by *tidal interactions* because the mass of the gas in the trail is more than three times larger than that contained in the elliptical. Had tidal interactions been at work, their effect would have been seen also in the distribution of the stars in NGC 6876. The isophotes of NGC 6876 are regular; Hubble Space Telescope observations do, however, reveal a slight central depression, which is not due to dust absorption. This has been interpreted as the possible signature of the end product of the merging of two gas-free stellar system, each harboring a massive black hole (Lauer et al. 2002). We can estimate the dynamical mass of NGC 6876 from the observed velocity dispersion of 231 km s^{-1} (Davies et al. 1987) using the relation $\left(\frac{M}{L}\right)_{\text{vir}} = (5.0 \pm 0.1) \times R_e \sigma_e^2 / (LG)$, which is the best-fitting virial relation found for a sample of 25 elliptical and lenticular galaxies from the SAURON sample (Cappellari et al. 2006). Taking the effective radius $R_e = 25.48 \text{ kpc}$ as the half-light radius in the blue-band given in NASA/IPAC Extragalactic Database, we obtain $M_{\text{vir}} = 1.57 \times 10^{12} M_\odot$. The projected distance on the sky between NGC 6872 and NGC 6876 is $\sim 142 \text{ kpc}$, and the radial velocity difference is about 800 km s^{-1} . This gives a timescale of 180 Myr, assuming comparable contributions from the velocity

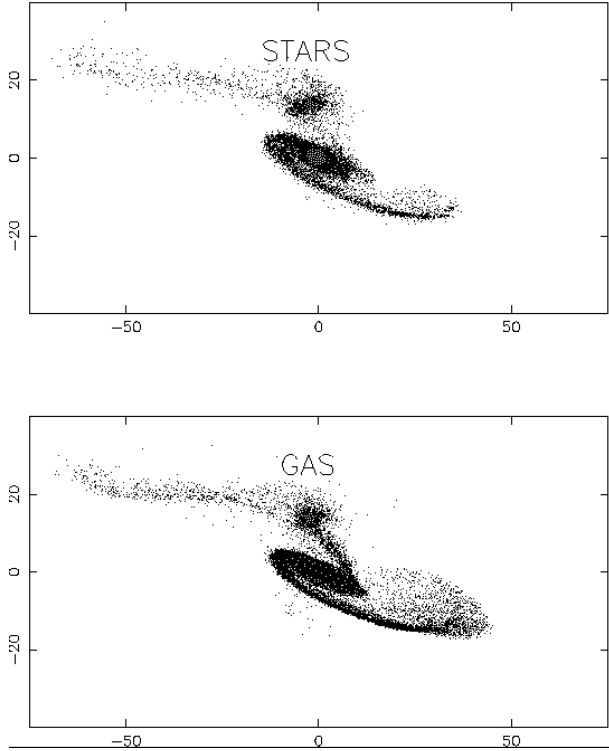


Fig. 8. Distribution the stars (top figure) and the gas (bottom figure) in the simulation 130 Myr after perigalacticon, when the simulated system resembles the observed one most. The position of the companion is indicated by a star.

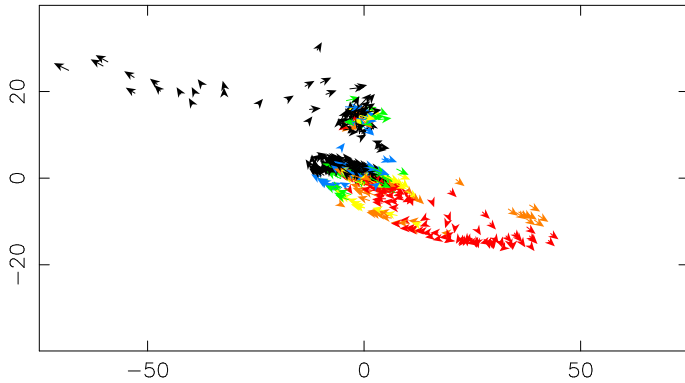


Fig. 9. Gas in the simulation 130 Myr after perigalacticon. The arrows indicate the direction of the velocity of the gas clouds projected on the plane of the sky. The colors indicate the velocity range along the line-of-sight, v_{los} : larger than 200 km s^{-1} in red, between 100 and 200 km s^{-1} in orange, between 0 and 100 km s^{-1} in yellow, between -100 and 100 km s^{-1} in green, between -200 and -100 km s^{-1} in blue, less than -200 km s^{-1} in black.

in the plane of the sky and the separation along the line-of-sight. If NGC 6872 had passed near NGC 6876, a $\sim 10^{12} M_{\odot}$ galaxy around 180 Myr ago, it is likely that such an interaction would have left a trace in the H α distribution, which is not observed.

– The X-ray trail could be due to *ram pressure stripping* from NGC 6872 as the spiral galaxy moves supersonically through the hot gas within the Pavo group (Machacek et al. 2005). Ram pressure stripping is known to affect the H α distribution in some galaxies (e.g. Vollmer et al. 2004). However, we do not see any

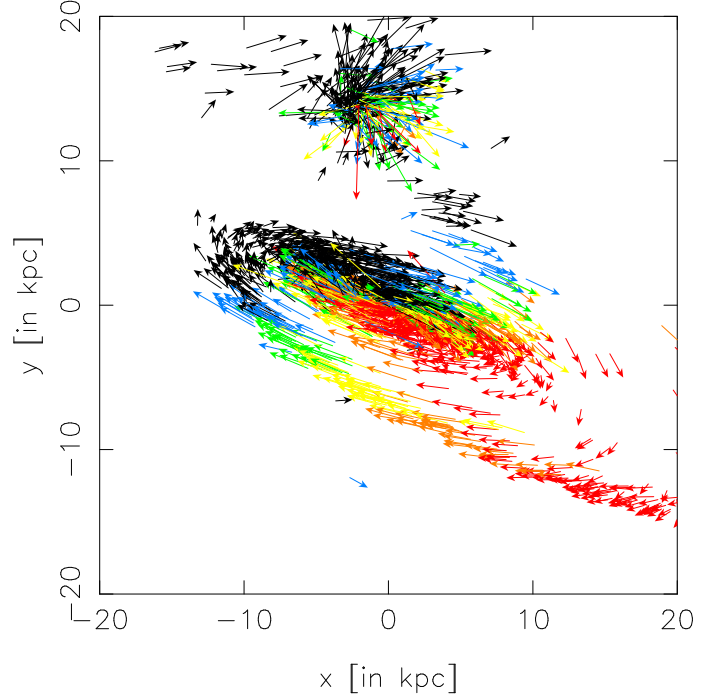


Fig. 10. Gas in the inner part of the simulated galaxy 130 Myr after perigalacticon. The length of the arrows is proportional to the velocity on the plane of the sky. The colors indicate the velocities along the line-of-sight, using the color code as in the previous figure.

sign of that effect in the observed H α distribution of NGC 6872. Therefore, we cannot infer any information about the motion of NGC 6872 with respect to the surrounding gas in the Pavo group.

– Other mechanisms involving an *interaction between the interstellar medium and the intergalactic medium* could be at work, such as turbulent viscous stripping (Nulsen 1982), where gas at the interface between the galaxy and the intergalactic medium could be heated. At the resolution of our H α observations, we do not see any evidence for that effect either.

– *Accretion into a Bondi-Hoyle trail* is the most favored hypothesis. Machacek et al. (2005) have calculated the extent of the trail assuming an NFW profile Navarro et al. (1996) for the dark matter distribution in NGC 6872 with a concentration parameter $c = 15$ and extending until a radius ca , where a is the inner radius. An extended halo, with an inner radius $a \approx 20 \text{ kpc}$, is required to reproduce the observed length of the trail. We have performed the same calculation, using a different profile for the halo, namely the one corresponding to the Plummer potential that we have used in the simulation with a scale length of 10 kpc . As illustrated in Fig. 11, for a Plummer profile the downstream profile of density contrast peaks at a larger distance from the moving halo, and decreases more softly. At a downstream distance $z = -10a$, the density contrast is slightly higher for the Plummer sphere than for the NFW profile. Although the density contrast along the trail is, in principle, sensitive to the density profile of the moving halo, this is difficult to use in practice. This calculation is simplified, based on linearized flow equations, which applies only for small density perturbations and Machacek et al. (2005) point out that the observed temperature ratio between the trail and the intra-cluster gas implies an overdensity larger than one.

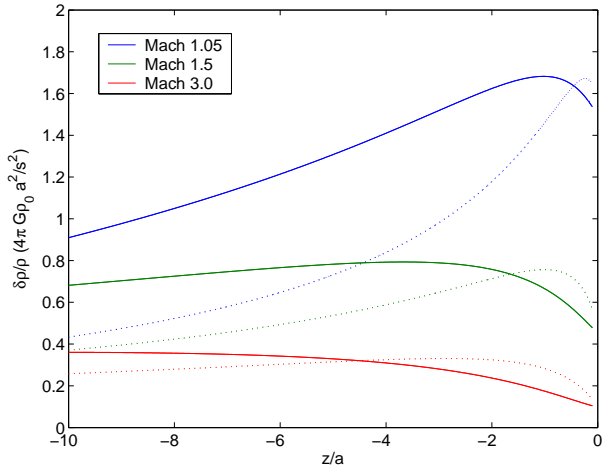


Fig. 11. Density contrast $\delta\rho/\rho$ downstream of a Plummer potential (solid lines) and an NFW potential (dotted lines) moving supersonically through a medium with different Mach numbers.

More sensitive X-ray observations would help elucidate the nature of the X-ray trail. As discussed above, gravitational interaction with the large elliptical is unlikely to have produced such an X-ray trail without any H α counterpart. More detailed simulations of the evolution of a spiral galaxy in the gravitational potential of a group, interacting with the hot intra-cluster medium and with both a massive elliptical and a smaller galaxy are required to shed more light on the relative importance of the different mechanisms. This is beyond the scope of this paper.

5. Summary and conclusion

In this paper we have presented interferometric H α observations of the interacting system NCG 6872/IC 4970 in the southern group of galaxies Pavo obtained with the ATCA, and N -body numerical simulations of the evolution of the system.

1. We detected about $1.54 \times 10^{10} M_{\odot}$ of H α gas toward the NGC 6872/IC 4970 pair, out of which about $1.3 \times 10^9 M_{\odot}$ is associated with the companion IC 4970. The gas in NGC 6872 is distributed in an extended rotating disk. Massive concentrations of gas ($\sim 10^9 M_{\odot}$) are found at the tip of both tidal tails and towards the break seen in the optical northern arm near the companion. An increased velocity dispersion is observed on each side of the galaxy's center, near the break in the northern arm and south of the main body where the southern tail starts; another region of higher velocity dispersion coincides with the most northern H α concentration. We have compared the H α distribution with that of stellar clusters observed by Bastian et al. (2005). Star clusters in the outer H α concentrations in the tails are predominantly young and low-mass (less than 100 Myr and less than $10^6 M_{\odot}$) and have a low extinction ($A_V < 1$).
2. No H α gas was found associated with the X-ray trail observed by Machacek et al. (2005) between NGC 6872 and NGC 6876, the dominant elliptical galaxy in the Pavo group located $\sim 8'$ to the southeast. However, as much as $\sim 3 \times 10^9 M_{\odot}$ of H α gas could be hidden in extended regions of diffuse emission below our detection limit. At the sensitivity and the resolution of the observations, there is no sign in the overall H α distribution that NGC 6876 has affected the evolution of NGC 6872. There is no evidence either of ram pressure stripping.

3. The simulations of a gravitational interaction with the small nearby companion IC 4970 on a low-inclination prograde passage are able to reproduce most of the observed features of NGC 6872, including the general morphology of the galaxy, the inner bar, the extent of the tidal tails and the thinness of the southern tail.
4. Our simulations do not model the gas environment within the group or the motion of NGC 6872 through the group. Without those interactions we cannot address the hydrodynamic processes, i.e. ram pressure stripping, turbulent viscous stripping, or Bondi-Hoyle accretion, discussed in Section 4. However, together with the H α maps, our simulations provide important constraints on viewing angle, internal velocities, mass and gas distributions for input into future hydrodynamic simulations.

Acknowledgements. We thank the referee for a very thoughtful report. We are grateful to Françoise Combes for providing us a version of the code, to Vassilis Charmandaris for his help with the VLT data, and to John Black for useful comments on the manuscript. We thank E. de Blok, E. Sadler and E. Muller for their help during the H α observations. We thank Chris Mihos for providing us his H α data and Nate Bastian for stimulating discussions. This research has made use of the NASA/IPAC Extragalactic Database (NED) which is operated by the Jet Propulsion Laboratory, California Institute of Technology, under contract with the National Aeronautics and Space Administration. The H α observations were done with the Australia Telescope Compact Array, which is funded by the Commonwealth of Australia for operations as a National Facility managed by the Commonwealth Scientific and Industrial Research Organisation (CSIRO).

References

- Arp, H. 1966, *ApJS*, 14, 1
 Arp, H. A. & Madore, B. F. 1987, Cambridge Univ. Press
 Bastian, N., Hempel, M., Kissler-Patig, M., Homeier, N. L., & Trancho, G. 2005, *A&A*, 435, 65
 Bik, A., Lamers, H. J. G. L. M., Bastian, N., Panagia, N., & Romaniello, M. 2003, *A&A*, 397, 473
 Bournaud, F., Duc, P.-A., Amram, P., Combes, F., & Gach, J.-L. 2004, *A&A*, 425, 813
 Bournaud, F., Duc, P.-A., & Masset, F. 2003, *A&A*, 411, L469
 Cappellari, M., Bacon, R., Bureau, M., et al. 2006, *MNRAS*, 366, 1126
 Davies, R. L., Burstein, D., Dressler, A., et al. 1987, *ApJS*, 64, 581
 Davoust, E. & Considere, S. 1995, *A&AS*, 110, 19
 de Vaucouleurs, G., de Vaucouleurs, A., Corwin, H. G., et al. 1991, Third Reference Catalogue of Bright Galaxies (Volume 1-3, XII, 2069 pp. 7 figs., Springer-Verlag Berlin Heidelberg New York)
 Dubinski, J., Mihos, J. C., & Hernquist, L. 1999, *ApJ*, 526, 607
 Elmegreen, B. G., Kaufman, M., & Thomasson, M. 1993, *ApJ*, 412, 90
 Green, M. R., Godwin, J. G., & Peach, J. V. 1988, *MNRAS*, 234, 1051
 Hibbard, J. E. & van Gorkom, J. H. 1996, *AJ*, 111, 655
 Holmberg, E. 1941, *ApJ*, 94, 385
 Horellou, C. & Booth, R. 1997, *A&AS*, 126, 3
 Horellou, C., Booth, R. S., & Karlsson, B. 1999, *Ap&SS*, 269, 629
 Horellou, C. & Koribalski, B. 2003, *Ap&SS*, 284, 499
 Horellou, C. & Koribalski, B. S. 2004, in *IAU Symposium*, ed. P.-A. Duc, J. Braine, & E. Brinks, 422
 James, R. A. 1977, *Journal of Computational Physics*, 25, 71
 Jarrett, T. H., Chester, T., Cutri, R., Schneider, S. E., & Huchra, J. P. 2003, *AJ*, 125, 525
 Johansson, L. & Bergvall, N. 1990, *A&AS*, 86, 167
 Larsen, S. S. & Richtler, T. 2000, *A&A*, 354, 836
 Lauberts, A. 1982, *ESO/Uppsala survey of the ESO(B) atlas* (Garching: European Southern Observatory (ESO), 1982)
 Lauer, T. R., Gebhardt, K., Richstone, D., et al. 2002, *AJ*, 124, 1975
 Machacek, M. E., Nulsen, P., Stirbat, L., Jones, C., & Forman, W. R. 2005, *ApJ*, 630, 280
 Meyer, M. J., Zwaan, M. A., Webster, R. L., et al. 2004, *MNRAS*, 350, 1195
 Mihos, J. C., Bothun, G. D., & Richstone, D. O. 1993, *ApJ*, 418, 82
 Moshir, M. & et al. 1990, in *IRAS Faint Source Catalogue*, version 2.0 (1990)
 Navarro, J. F., Frenk, C. S., & White, S. D. M. 1996, *ApJ*, 462, 563
 Nulsen, P. E. J. 1982, *MNRAS*, 198, 1007
 Pfeleiderer, J. 1963, *Zeitschrift für Astrophysik*, 58, 12
 Pfeleiderer, J. & Siedentopf, H. 1961, *Zeitschrift für Astrophysik*, 51, 201

- Russell, J. L., Lasker, B. M., McLean, B. J., Sturch, C. R., & Jenkner, H. 1990, AJ, 99, 2059
- Skrutskie, M. F., Cutri, R. M., Stiening, R., et al. 2006, AJ, 131, 1163
- Spitzer, L. J. 1942, ApJ, 95, 329
- Springel, V. & White, S. D. M. 1999, MNRAS, 307, 162
- Toomre, A. 1964, ApJ, 139, 1217
- Toomre, A. & Toomre, J. 1972, ApJ, 178, 623
- Vollmer, B., Balkowski, C., Cayatte, V., van Driel, W., & Huchtmeier, W. 2004, A&A, 419, 35